Available online at www.sciencedirect.com
ScienceDirect
International Journal of Heat and Mass Transfer 51 (2008) 835–843
International Journal of HEAT and MASS TRANSFER
www.elsevier.com/locate/ijhmt

Experimental study of drag-reduction mechanism for a dilute surfactant solution flow

Feng-Chen Li [a,*], Yasuo Kawaguchi [b], Bo Yu [c], Jin-Jia Wei [d], Koichi Hishida [e]

[a] School of Energy Science and Engineering, Harbin Institute of Technology, Harbin 150001, China
[b] Department of Mechanical Engineering, Tokyo University of Science, Yamazaki 2641, Noda, Chiba 278-8510, Japan
[c] Beijing Key Laboratory of Urban Oil and Gas Distribution Technology, China University of Petroleum (Beijing), Beijing 102249, China
[d] State Key Laboratory of Multiphase Flow in Power Engineering, Xi'an Jiaotong University, Xi'an 710049, China
[e] Department of System Design Engineering, Keio University, Yokohama 223-8522, Japan

Received 30 November 2006; received in revised form 19 April 2007
Available online 26 July 2007

Abstract

The quantitative characteristics of vortex structures and turbulent events in turbulent channel flows with and without drag reduction were investigated experimentally. Drag reducing aqueous solutions of CTAC (CTAC – cetyltrimethyl ammonium chloride) with concentration of 25 ppm and 75 ppm at 30 °C were tested. Particle image velocimetry (PIV) was used to measure the instantaneous velocity field in the streamwise–wall-normal plane of the flow. Through visualizing the instantaneous vector fields, contour maps of the swirling strength and instantaneous value of uv (u and v are the streamwise and wall-normal velocity fluctuations, respectively), the characteristic angle of vortex packets was quantified. It was shown that the drag-reducing CTAC additive reduced both the strength and frequency of turbulent bursts near the wall, and the characteristics of vortex structures and bursts were not only dependent on drag-reduction level but also on concentration of additive. From the quantified parameters characterizing turbulent events in a wall-bounded turbulent flow, it was obtained that f_T was linearly proportional to the product of frequency and strength of turbulent events.

Keywords: Drag reduction; Channel flow; Surfactant solution; Turbulent events; PIV

1. Introduction

Adding a minute amount of drag-reducing polymer or surfactant additives may cause a dramatic frictional drag reduction (DR). This drag-reducing effect has great potentials in the industrial applications, such as in saving pumping power in a water-circulating device like a district heating/cooling system. For such applications, surfactant additives are more suitable than polymer due to its quick self-repairing ability after the mechanical degradation caused by pump. Both drag-reducing polymer and surfactant solution flows behave viscoelastic characteristics. The most notable elastic property of the viscoelastic polymer or surfactant solutions is that stress does not immediately become zero when the fluid motion stops, but rather decays with some characteristic time (the relaxation time), which can reach seconds and even minutes. It is generally believed that the frictional DR caused by surfactant additives in a wall-bounded flow is the consequence of the interaction between viscoelasticity and turbulence in the flow. In a cationic surfactant solution, rod-like micelles can be formed if the surfactant/counterion chemical structures, molar ratios, concentrations and temperature are under right conditions. This network microstructure imparts viscoelasticity to the solution flow, which was often stated to be responsible for the occurrence of DR [1,2].

The present work is one of the continuous experimental studies on drag-reducing surfactant solution flow using

* Corresponding author. Fax: +86 451 86413254.
E-mail addresses: lifch@hit.edu.cn (F.-C. Li), yasuo@rs.noda.tus.ac.jp (Y. Kawaguchi).

0017-9310/$ - see front matter © 2007 Elsevier Ltd. All rights reserved.
doi:10.1016/j.ijheatmasstransfer.2007.04.048

Nomenclature

F	frequency of turbulent burst	v	wall-normal velocity fluctuation (m/s)
f_T	turbulent contribution to frictional drag coefficient	x	coordinate in the streamwise direction (m)
H	channel height (m)	y	coordinate in the wall-normal direction (m)
N	number of coherent structures	z	coordinate in the spanwise direction (m)
N_f	number of PIV frames	*Greek symbols*	
$\bar{n}$	population density of coherent structure	λ	relaxation time (s)
P	strength of turbulent burst	λ_{ci}	swirling strength (1/s)
Re	Reynolds number based on bulk velocity, channel height and water viscosity	γ	inclination angle of near-wall coherent structure (deg)
U_b	bulk velocity (m/s)	υ	kinematic viscosity (m^2/s)
u	streamwise velocity fluctuation (m/s)	$\bar{\gamma}$	average angle of coherent structures (deg)
u_τ	friction velocity (m/s)	ω_z	spanwise vorticity (1/s)

particle image velocimetry (PIV). Since the occurrence of DR is basically due to the interaction of viscoelasticity with turbulent eddies in the flow, our studies have focused on investigating the influence of drag-reducing surfactant additives on the turbulent bursting events and the turbulence structures particularly in the near-wall region of a channel flow. The spatial structure of turbulence in a drag-reducing channel flow with surfactant additives was investigated in [3]. It was obtained that, for a 40 ppm CTAC (cetyltrimethyl ammonium chloride) solution flow with 60% DR, the penetration from the low-speed fluid region into the high-speed region, which is one of the important events of turbulence energy production and turbulent mixing, disappeared as compared with a water flow at the same Reynolds number (*Re*). Furthermore, the strong vorticity fluctuation near the wall disappeared in the drag-reducing flow and the probability of "Eddy" and "Convergence" (a classification given in [4]), which accompany vortex motion largely disappeared near the wall. The two-dimensional three-component velocity field in both the streamwise-spanwise and wall-normal-spanwise planes of a drag-reduced channel flow (DR = 54%) with CTAC additives was measured using a stereoscopic PIV [5]. A three-dimensional image of the vortex tubes or the hairpin vortex leg(s) inclined toward the wall was obtained through analysis of the velocity fields in both planes. The conditionally averaged wall-normal vorticity and turbulence intensity of wall-normal velocity were decreased in the buffer layer by about one order of magnitude by the drag-reducing additives, while they were in the same order in the outer region for both water and solution flows, indicating that suppression of turbulence in the buffer layer could be the most effective one in reducing the overall skin friction for a wall-bounded turbulent flow. The Re dependence of turbulence structures in a drag-reducing surfactant solution channel flow was investigated by means of PIV in [6]. From the analysis of the PIV-measured velocity field in the streamwise–wall-normal plane at different *Re* (different *Re*-dependent regions have been categorized based on the variation trend of DR levels with the *Re*), the relationship between the dynamic processes of the shear-induced structures in the solution and the turbulence structures quantified by the turbulence statistics was revealed in an indirect way. Very recently, we reported in a Letter a simple correlation for the turbulent contribution to frictional drag coefficient (f_T) in a wall-bounded turbulent flow: f_T in a wall-bounded turbulent flow is linearly proportional to the product of spatial frequency and strength of the turbulent bursts originated from the wall [7]. The present study would contribute to stress the details of the PIV experiments, detailed analysis of the quantification of turbulent bursting events and the near-wall coherent vortex structures in turbulent channel flows with and without DR, and elaboration of the deduction and verification of the correlation for f_T as previously proposed [7]. The mechanism of DR for a drag-reducing surfactant solution channel flow was then revealed from the viewpoint of quantification of turbulent bursts.

From analytical and experimental studies by means of direct numerical simulation (DNS) and flow visualization including PIV, respectively, the mechanism of wall turbulence has been established based on a hierarchy of hairpin vortex packets [8–12]. The central element of the mechanistic model is the hairpin vortex; a second central element is the packet of hairpins; and the third is an auto-generation process whereby a hairpin vortex spawns a younger, smaller hairpin, which in turn spawns a still younger hairpin [13]. The heads of the sequence of older to younger hairpins that form a packet are observed to form a characteristic angle with respect to the wall (between 12° and 20° in DNS by Zhou et al. [9], 12° on average in PIV measurement by Adrian et al. [10], and 20° in flow visualization using smoke by Head and Bandyopadhyay [14]). The evolution of vortex packets has a close relationship with the bursting events in wall turbulence. Ejections of low-momentum fluid from the wall (Q2 motion, Q means quadrant) are associated with the flow induced by the head and neck of a hairpin vortex (below the vortex head),

and sweeps of high-momentum fluid toward the wall (Q4 motion) happen in a region in the downwash of an upstream hairpin vortex, or when an eddy propagates more slowly than the surrounding fluid [10]. Furthermore, the streamwise spacing of vortex packets is related to the frequency of the bursting event.

Essentially, all of the turbulent kinetic energy and most of the turbulent transport occurs during bursting events associated with the ejection and sweep motions [15,16], and the fluid motions during bursts generate principal contributions to the Reynolds shear stress. The drag-reducing ability of any additives is directly associated with the ability of influencing vortex structures and bursting events. Indeed, it has been observed that the frequency of bursts decreased for drag-reducing dilute polymer solution flows, and compared to a water flow at the same wall shear stress, the increase in the timescale between bursts was equal to the increase in the average low-speed-streak spacing [17,18]. The turbulent contribution to frictional drag, f_T, in a wall-bounded turbulent flow is an embodiment of the bursting events through the term of the Reynolds shear stress [19]

$$f_T = \frac{6}{U_b^{+2}} \int_0^1 (1 - y^*)\tau_t^+ \, dy^* \tag{1}$$

where $y^* = y/(H/2)$, $\tau_t^+ (= -\overline{u^+ v^+})$ is the turbulent shear stress, and the superscript "+" denotes normalization with u_τ. The principal parameters characterizing bursting events in a wall-bounded turbulent flow are the frequency, F, and strength, P, of bursts. We therefore postulate that

$$f_T \propto \overline{F} \cdot \overline{P} \tag{2}$$

where the overbar means average value.

In this study, the characteristics of vortex structures and turbulent events in a channel flow of water with and without surfactant additives (with and without DR) were investigated by means of visualization of the turbulent velocity field and identification of vortices. The penetration behavior of low-speed fluid into the high-speed region as found in the previous study was quantified for both water flow and drag-reducing flows, and the identification of vortices was based on the swirling strength instead of vorticity, as described later. Through analysis of the quantified parameters characterizing turbulent events in a wall-bounded turbulent flow, the postulated correlation of turbulent contribution to the friction factor was verified.

2. Experimental facility

The experiment was performed on a closed-circuit water loop. The test section was a two-dimensional channel made of transparent acrylic resin having a length of 10 m, height (H) of 0.04 m and width of 0.5 m. A honeycomb rectifier with length of 0.15 m was set at the channel entrance for removing large eddies. An electromagnetic flow meter with uncertainty of ± 0.01 m^3/min was installed upstream of the channel for measuring the flow rate. The liquid-supplying tank in the flow loop contained cooling coils and a heater, which maintained a fluid temperature of 30 °C for the present purpose with uncertainty of ± 0.1 °C. The wall shear stress was estimated from the static pressure gradient, which was measured with pressure tabs located on the bottom wall of the channel over a distance of 1.5 m with uncertainty of ± 0.1 Pa. For details of the experimental facility, one refers to [6].

The surfactant tested in this experiment was the cationic surfactant, cetyltrimethyl ammonium chloride (CTAC). Local tap water was used as the solvent. Sodium salicylate (NaSal) was added to the solution with the same weight concentration as that of CTAC for providing counterions. For simplicity, hereinafter, the surfactant solution is only designated as CTAC concentration. 25 ppm and 75 ppm CTAC solutions at 30 °C were used as the drag-reducing fluid. The rheology-measurement (ARES Rheometer, Rheometrics Scientific F.E. Ltd., Japan for the measurement the shear-viscosity and the storage and loss moduli, and a RFX Rheometer, Rheometrics Inc., USA for the measurement of the extensional viscosity) indicated that only 75 ppm CTAC solution showed distinct rheological properties, i.e., shear-rate (extensional strain-rate) dependent shear-viscosity (extensional viscosity) [20]; the measured properties of 25 ppm CTAC solution were almost the same as those of water at the same temperature, as shown in Fig. 1 for the profiles of shear-viscosity. The relaxation time (λ) for 75 ppm CTAC solution (Table 1) was obtained by means of the best-fit method with the aid of the viscoelastic constitutive model [20]. Since both solutions exhibited effective drag-reducing ability at appropriate Reynolds number range and it has been commonly

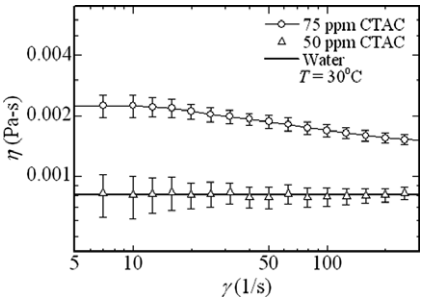

Fig. 1. Shear-viscosity as a function of shear-rate (no visible difference for 25 ppm CTAC solution from water).

Table 1
Flow parameters

Cases	Fluid	λ (s)	Re ($\times 10^4$)	u_τ (m/s)	DR (%)
W	Water	0	1.8	0.020	–
C1	CTAC, 25 ppm	>0	2.6	0.026	10
C2	CTAC, 25 ppm	>0	2.1	0.019	34
C3	CTAC, 25 ppm	>0	1.3	0.010	58
C4	CTAC, 75 ppm	0.1	1.1	0.009	51

accepted that the drag-reducing ability is due to viscoelasticity, we supposed that the relaxation time for 25 ppm CTAC solution should be larger than zero (Table 1). The fluid properties of the solvent at mean fluid temperature were used for data reduction. Local tap water was also used as the working fluid for comparison.

3. PIV measurement and data reduction

The PIV system consisted of a double-pulsed laser, laser sheet optics, charge-coupled device (CCD) camera, timing circuit, image-sampling computer and image-processing software (TSI Insight ver. 3.3). The double-pulsed laser (New Wave Research Co. Ltd., MiniLase-II/20 Hz) is a combination of a pair of Nd-YAG lasers, each having an output of 25 mJ/pulse and maximum repetition rate of 20 Hz. By changing the combinations of the cylindrical lenses, the laser sheet thickness can be modified from 0.14 to 0.6 mm and beam spread angle from 4.3° to 13.3°. The timing circuit (TSI Model 610032) communicates with the CCD camera and computer, and generates pulses to control the double-pulse laser. The CCD camera used (PIVCAM 10-30, TSI Model 630046) has a resolution of 1280 × 1024 pixels.

Fig. 2 shows a schematic of the optical configuration for PIV measurement on a streamwise–wall-normal (x–y) plane. Cartesian coordinates are also shown in the diagram. The measurement position was located at 7.0 m (175H) downstream of the channel entrance. The laser sheets were aligned at $z = 250$ mm ($z = 0$ at the side-wall) for the x–y plane measurements. Measurements were performed for one case of water and four cases of CTAC solution flows. Details of the flow parameters are shown in Table 1.

PIV images were acquired for 200 dual frames (400 double-exposed PIV photographs) for all the measurements. The photograph acquisition rate was 8 Hz, indicating that the velocity field was recorded at 4 Hz. For the x–y plane measurements, the picture frames were all taken to cover the full height of the channel (the PIV image covered an area of about $x \times y = 52 \times 42$ mm^2). The interrogation area was set to be 32 × 16 pixels (with 50% overlap in each direction) for velocity vector analyses. The spacing between adjacent vectors in each direction was around $\Delta x = 0.65$ mm, $\Delta y = 0.33$ mm, respectively. Resolutions of the PIV measurements are listed in Table 2. The tracer particles used to seed the flow were acrylic colloid with a diameter of 0.1–1 μm. The particle concentration was adjusted so that on average at least 10 particle pairs were observed in an interrogation window for each case.

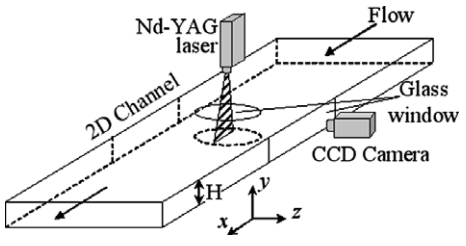

Fig. 2. Optical configuration for PIV measurement.

Table 2
Resolution of the PIV experiments

Case	W	C1	C2	C3	C4
$\Delta x^+ (= u_\tau \Delta x/\upsilon)$	16.1	20.9	15.3	8.1	7.2
$\Delta y^+ (= u_\tau \Delta y/\upsilon)$	7.4	9.6	7.0	3.7	3.3

The procedure of extracting velocity vectors from the PIV photographs performed in the present experiments was similar to that in [6,10]. After a vector field had been calculated by interrogating a dual frame, it was validated to remove erroneous velocity vectors that might have been detected incorrectly during interrogation owing to random noise in the correlation function, accomplished by the TSI Insight software. Empty data cells (holes) occurred after erroneous velocity vectors were removed. A FORTRAN program was made for filling holes in the vector field by interpolation of neighboring velocity vectors. The program was also used for applying a Gaussian filter to the velocity field and calculating the ensemble turbulence statistics. A round Gaussian kernel whose e^{-2} radius was 80% of the vector grid spacing was used to filter the two-dimensional velocity vector field so that white noise was removed.

4. Results and discussion

In this section, we present the characteristics of vortical structures, turbulent events and the Reynolds shear stress contributions in the drag-reducing surfactant solution flows, based on the PIV measurement of turbulent velocity field in the streamwise–wall-normal plane. In the velocity-vector plots shown in the following sections, Reynolds decomposition (the local mean velocity is subtracted from the vectors) has been performed to clearly illustrate low- and high-momentum zones. In addition, the swirling strength was used to identify the vortex cores. The swirling strength, λ_{ci}, is defined as the magnitude of the imaginary part of the eigenvalue of the local velocity gradient tensor. For a planar velocity field measured by PIV, only the in-plane gradients were used to form a two-dimensional tensor. Vortices were then identified by extracting iso-regions of λ_{ci} [5,21], as shown in relative figures.

4.1. Vortical structures and turbulent events influenced by drag-reducing additives

Fig. 3 shows an example of a snapshot velocity field for five cases, W and C1–C4, respectively. Together with the contour map of swirling strength, the vortical structures can be figured out from the velocity vectors. Except for the case of C4, vortex packets, formed by a sequence of vortices, can be observed and the heads of the vortex in a packet show a growth angle with respect to the walls.

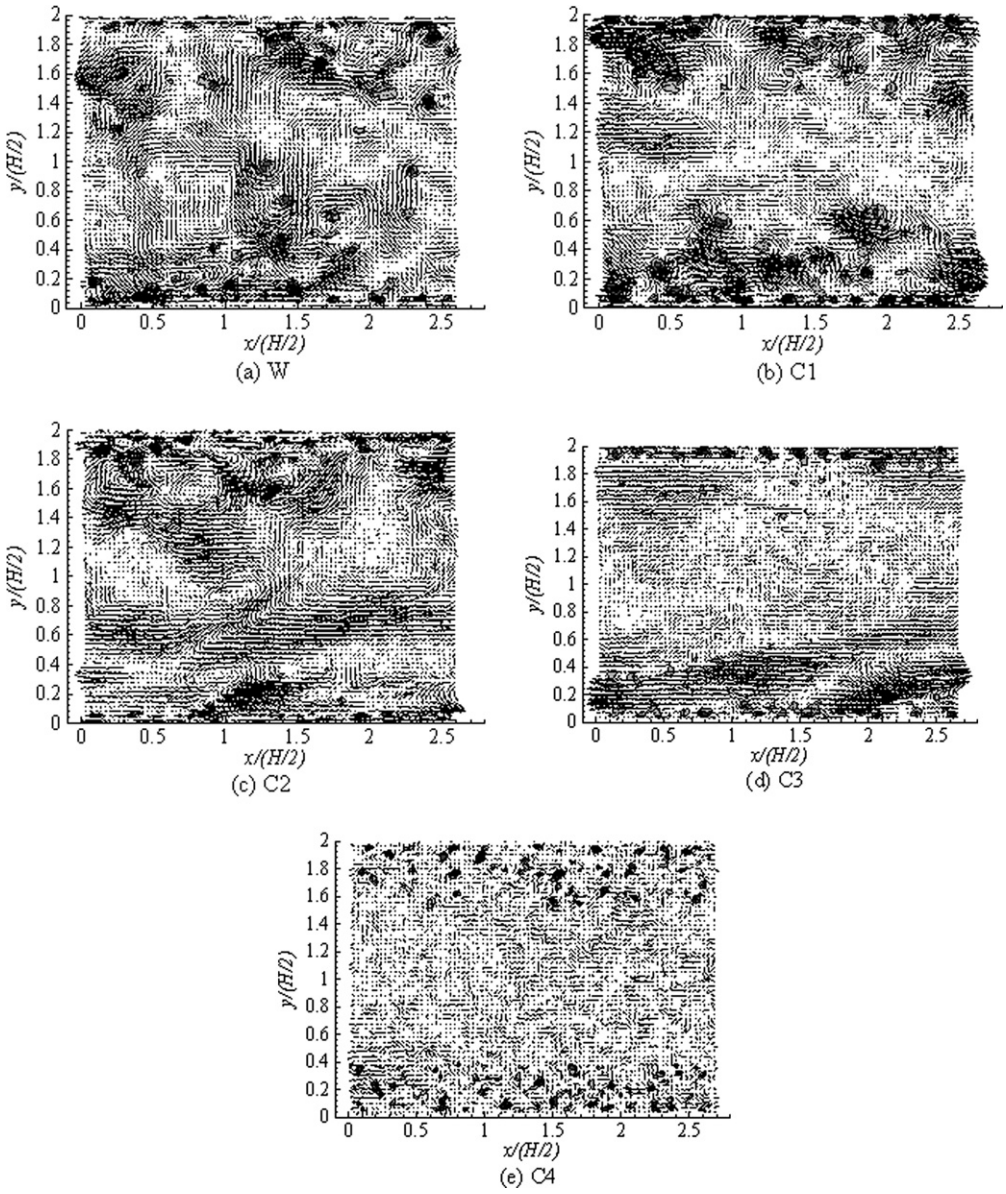

Fig. 3. Instantaneous velocity field and vortex structures (flow is from left to right).

The vortex packet growth angle also appears as the inclination angle of the ramp-shaped low-momentum regions (penetration of low-speed fluid into high-speed region [3]) covered by the vortex footprint, as shown in Fig. 3(a)–(d).

As we have shown, the structures of vortex packets near the walls are associated with bursting events. A strong Q2 motion may penetrate into the core region at a high rate. On the other hand, in a DNS study [9], it was observed that the auto-generation process of the primary hairpin vortex forming secondary and tertiary hairpin vortices showed a threshold behavior, i.e., only in the case of strong initial vortex structures was the auto-generation process possible. Weak vortices are either convected downstream by themselves or annihilated during convection, forming the ramp-shaped low-momentum region with a gentler angle of. From this phenomenon, we suppose that the growth angle of the vortex packet may characterize the strength of bursts.

Compared with water flow (Fig. 3a), it is observed that the near-wall vortex structures near the walls in the drag-reducing surfactant solution flow are changed gradually with DR level: the growth angle of vortex packets or inclination angle of the ramp-shaped regions decreases, and the appearance of coherent vortex structures becomes less frequent.

By visualizing the instantaneous velocity field, we extracted the near-wall vortex structures and measured the growth angle (or inclination angle) γ or in other words, the strength of turbulent burst. Fig. 4 shows an example of the extraction of coherent structure. Each circle designates the existence of a vortex head, and between those vortex heads and wall surface a low-momentum

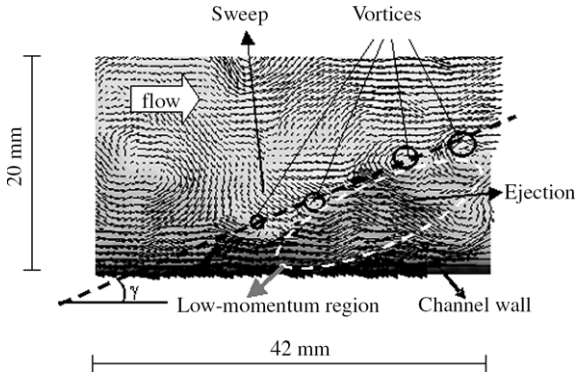

Fig. 4. An example of extraction of coherent structure.

region is formed locally. Such coherent structure is then extracted and the inclination angle or growth angle γ is measured. A coherent structure is judged by three obvious features: (1) ramp-shaped low-momentum region near the wall appearing in the contour map of streamwise velocity; (2) existence of vortex/vortices covering the low-momentum region; (3) apparent ejection/sweep motions in and over the low-momentum region. To identify the existence of vortex core, the contour of swirling strength (λ_{ci}) was use as a flag (as shown in Fig. 3). Visualization was made on 200 frames and near both walls. For water flow W, 232 vortex packets or low-momentum ramps were obtained; for CTAC solution flows, 186, 153 and 58 vortex packets were obtained for C1, C2 and C3, respectively; however, for flow C4, no obvious coherent structures were found, or we can say the growth angle of the coherent structures was 0° for the flow C4. Note that in the present PIV-experimental study, it was really hard to obtain a sufficient number of vortex packets statistically relevant, since the vortex packets were distinguished from each PIV-frame manually instead of automatically. Nevertheless, we still think that it was meaningful to do some simple statistical analysis like averaging and calculating the probability density function. Fig. 5 shows the probability density function of the inclination angle, PDF(γ), for the cases of W and C1–C3. The lines in the figure are fitted curves of experimental data for each case using least-squared method. It can be seen that the convex portion of the curve of PDF(γ) moves towards small inclination angle with DR level, which means that the most common characteristic inclination angle of near-wall vortical structures in drag-reducing flow is lowered. This indicates the inhibition of bursting events by drag-reducing additives. The average inclination angle in flows W, C1–C3, were 20.0°, 16.0°, 13.2° and 7.5°, respectively. The decrease of the number of extracted coherent vortex structures in drag-reducing flow means a decrease of frequency of bursts (strong enough and visible in the above-mentioned visualization) in a statistical sense. For example, the bursting frequency for flow C3 should be less than 25% of that for flow W, so combined with the reduction of the strength of bursts, a 58% reduction of frictional drag was thus obtained.

On the other hand, comparing flow C4 (75 ppm CTAC solution) with flow C3 (25 ppm CTAC solution), the vortex structures near the wall exhibit different behaviors irrespective of similar DR levels and similar Reynolds numbers. It is therefore expected that the characteristics of vortex structures and occurrence of bursting events in a drag-reducing flow by additives are not only dependent on DR level, but also dependent on solution concentration or viscoelasticity (viscoelasticity increases with concentration of additives), even for the same type of surfactant additive. This issue will be discussed again in latter section.

Fig. 6 shows the mean spanwise vorticity ω_z, which is weighted by λ_{ci} and normalized by $(H/2)/u_\tau$. In this form, only the vorticity at locations where swirling motions exist is sampled. It is seen that the weighted vorticity in drag-reducing surfactant solution flows, as compared with water flow, is greatly decreased and the peak value moves towards the wall as DR level increases. These are consistent with the observations on vortical structures near the wall as illustrated previously.

4.2. Reynolds shear stress distribution influenced by drag-reducing additives

From quadrant analysis of instantaneous velocity field, it is well known that the contributions from Q2 and Q4 motions during bursting events in wall turbulence are dominant in the Reynolds shear stress [22–24]. The frictional drag in a wall-bounded turbulent flow is closely associated with the bursting events through the weighted integration of the Reynolds shear stress across half of the flow passage.

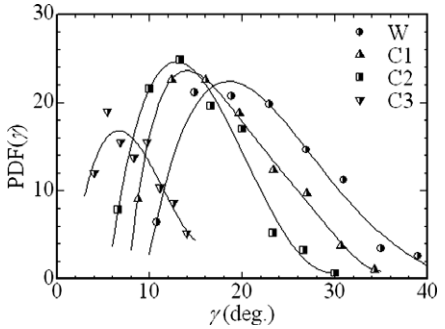

Fig. 5. Probability density function of the growth angle of vortex packets.

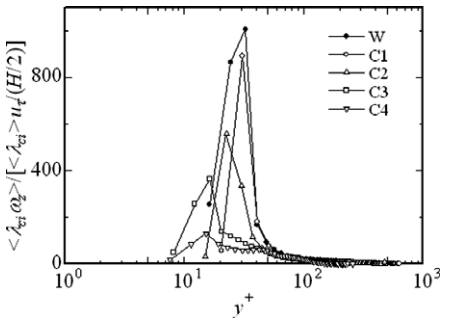

Fig. 6. Profiles of the average vorticity weighted by swirling strength.

Hence, the drag-reducing ability of additives is at last reflected on how much the additive influences on the Reynolds shear stress and its distribution across the flow passage.

Fig. 7 shows the contour maps of uv/u_τ^2 for the five cases. It is clearly seen from Fig. 7(a) for water flow that the large-amplitude uv/u_τ^2 only concentrates on several patches where the Q2 or Q4 motion occurs. The amplitude of uv/u_τ^2 is evidently small in large areas other than such patches. For 25 ppm CTAC solution flows, the area of patches with large uv-amplitude shrinks and the amplitude of uv/u_τ^2 on such patches decreases on average (judged by the same contour level with water flow) with DR level from C1 to C3. Note that, what is shown in Fig. 7(d) is only a single example, since such clearly-shaped coherent structures are very few for flow C3, as stated in last section. For 75 ppm CTAC solution flow, C4, the contour map of uv/u_τ^2 shows rather different characteristics from others: no patches with large uv-amplitude are observed, consistent with the fact that no obvious coherent structures were extracted for this case, but many spots with 'large' value of uv/u_τ^2 (compared with water flow, the value is quite small) are dispersed across the channel height.

As a consequence of the influence of surfactant additives on the Reynolds shear stress distribution, the ensemble value of $-\overline{u^+v^+}(=-\overline{uv}/u_\tau^2)$ is decreased in drag-reducing flows, as shown in Fig. 8. Interestingly, it is noted that the Reynolds shear stress decreases more in flow C4 than in flow C3, though the DR for flow C4 (51%) is slightly lower than that for flow C3 (58%). It is thus evident that the turbulent structure influenced by drag-reducing additives is not only dependent on DR level, but also on the concentrations of additives (or the rheological properties of the solution). For a surfactant solution flow, in addition to the viscous and turbulent contributions, elasticity of the solution imparts the elastic contribution to the frictional

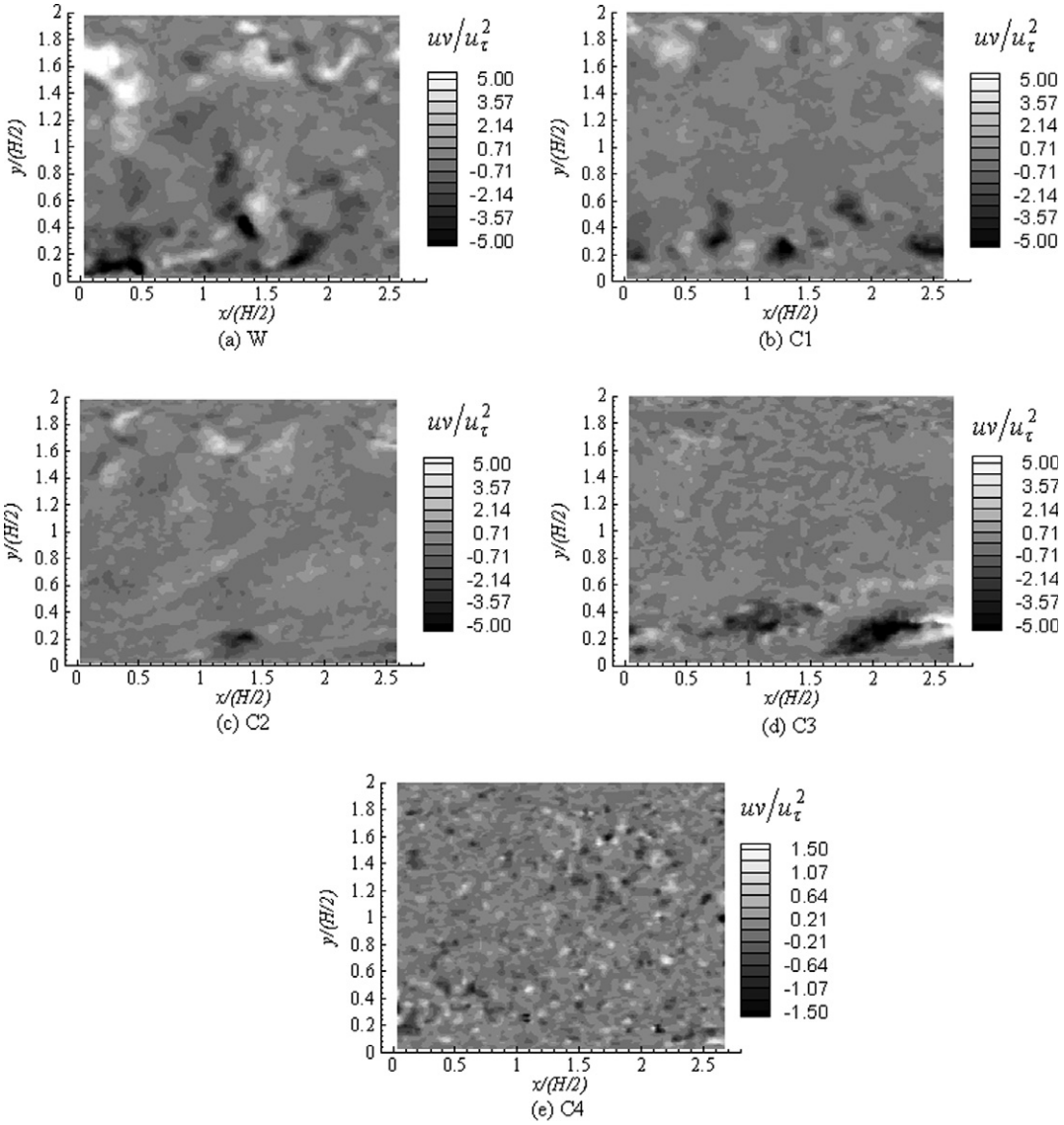

Fig. 7. Instantaneous velocity field and contour map of uv.

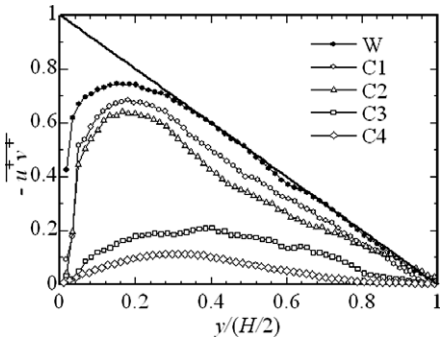

Fig. 8. Profiles of average Reynolds shear stress.

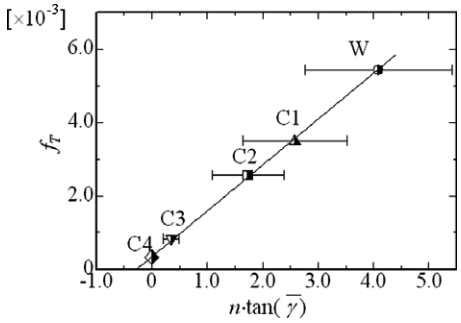

Fig. 9. Turbulent contribution to friction factor as a function of population density of coherent structure and inclination angle.

drag [6]. This additional contribution is expected to be larger for flow C4 than for flow C3, due to larger elasticity at higher concentration of additives. This may explain the fact the Reynolds shear stress decreases more but DR is lower for flow C4 compared with C3.

5. Quantitative relationship between turbulent contribution to friction factor and turbulent events

The essential characteristic of a wall-bounded turbulent flow, as compared with a laminar flow, is the occurrence of turbulent bursting events originated from the wall intermittently. The intermittent bursting events generate a statistically averaged turbulent contribution to the friction factor, which is much larger than its laminar counterpart. For a drag-reducing surfactant solution flow, there is an additional contribution to the friction factor, i.e., elastic contribution, due to viscoelasticity imparted into the solution by surfactant additives. As shown in the previous sections, the additives inhibit turbulent events (frequency and strength), and reduce the Reynolds shear stress and the turbulent contribution to the friction factor, and hence cause DR.

Control of wall-bounded turbulence is equivalent to control of turbulent bursting events, and of the turbulent contribution to the friction factor, f_T, in the final analysis. It is therefore natural to straightforwardly correlate f_T, which can be obtained from the Reynolds shear stress through Eq. (1), with the principal characteristic parameters of turbulent events. We have extracted coherent structures containing vortex packet(s) from a number of separate PIV frames ($N_f = 200$) for all the flows. In a statistical sense, we suppose that the number of extracted coherent structure, N, from N_f frames is equal to the number of coherent structure in a streamwise distance of $\Delta L = \Delta x \cdot N_f$, where Δx is the streamwise length of each PIV frame. Hence, $\bar{n} = N/(2\Delta L)$ represents the population density of coherent structure in the streamwise direction on one wall, playing an analogous role to the occurrence frequency of bursts. The strength of turbulent events can be characterized by the inclination angle of coherent structure, γ: a strong Q2 motion can penetrate into the core region at a high rate, resulting in a steep inclined slope, $\tan(\gamma)$, of a ramp-shaped low-momentum region below the vortex packets. Strong bursting events, involving vortices with large strength, are characterized by large penetration depth, and so accompanied with sweep motion by fluid at higher speed.

We have obtained the three terms of f_T, $\bar{n}$ and γ, as elucidated in the former sections, which allow us to investigate the quantitative relationship between turbulent contribution to friction factor and the characteristic parameters of turbulent events. Fig. 9 plots f_T versus $\bar{n} \cdot \tan(\bar{\gamma})$ for the five cases, where $\bar{\gamma}$ is the mean value of γ for each case. It is striking to see that f_T shows a perfect linear relationship with the term $\bar{n} \cdot \tan(\bar{\gamma})$. For the flow C4, we did not extract any clear coherent structures, or $\bar{\gamma} = 0$. Thus, the following equation is proposed

$$f_T - f_T|_{\bar{\gamma}=0} = C \cdot \bar{n} \cdot \tan(\bar{\gamma}) \tag{3}$$

here $C = 1.3 \times 10^{-3}$ is obtained. Since the correlation (Eq. (3)) is obtained based on the idea of assuming turbulent events to be energy quanta, we suppose that it could also apply to other drag-reducing flows. The mechanism of the turbulent contribution to the friction factor is schematically illustrated in Fig. 10 for wall-bounded flow [7–10]. The near-wall coherent structures or vortex packets associated with turbulent bursting events have been considered as many energy quanta, and the energy quanta in an integration fashion contribute to frictional drag coefficient in a turbulent wall flow. The drag-reducing surfactant additives inhibit turbulent bursts and decrease the strength and occurrence frequency of such energy quanta, resulting in a great decrease of turbulent contribution to frictional drag and DR.

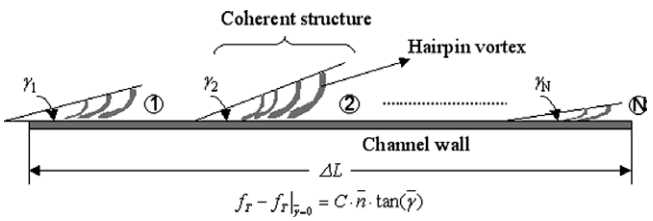

Fig. 10. Schematic illustration of the mechanism of turbulent contribution to friction factor. $\bar{n}$ represents the population density of coherent structure in the streamwise direction, and $\tan(\bar{\gamma})$ characterizes the strength of turbulent event.

6. Conclusions

The following conclusions are drawn from this study:

(1) The growth angle of vortex packets or the inclination angle of the low-momentum region below a hairpin vortex, and the frequency of bursts, were decreased in drag-reducing flow, indicating that the additive inhibited bursting events. The vorticity was decreased and the peak value moved towards the wall with DR level.
(2) The influenced vortex structures not only depended on DR level, but also depended on the concentration of the solution, even for the same surfactant additive.
(3) Across the channel height, the area of patches where bursting motions occurred was reduced, and the amplitude of instantaneous uv at such patches was also decreased, causing a reduction of the ensemble value of the Reynolds shear stress in drag-reducing surfactant solution flow, and hence drag reduction.
(4) A correlation of turbulent contribution to the friction factor in a wall-bounded turbulent flow was proposed: f_T is linearly proportional to the product of frequency and strength of turbulent events, which has been verified by the experimental result.

Acknowledgements

This research was carried out as a research project of the Center for Smart Control of Turbulence with financial support by the Ministry of Education, Culture, Sports, Science and Technology (MECSST), Japan. This work was partially supported by Harbin Specialized Research Fund for Scientific Technology Innovation (No. 2006RFLXS013). The third author wishes to acknowledge the support from the National Natural Science Foundation of China (No. 50506017). The fourth author wishes to acknowledge the financial support from the National Natural Science Foundation of China (Nos. 50521604, 10602043).

References

[1] J.L. Zakin, J. Myska, Z. Chara, New limiting drag reduction and velocity profile asymptotes for nonpolymeric additives systems, AIChE J. 42 (1996) 3546–3554.
[2] B. Lu, X. Li, L.E. Scriven, H.T. Davis, Y. Talmon, J.L. Zakin, Effect of chemical structure on viscoelasticity and extensional viscosity of drag-reducing cationic surfactant solutions, Langmuir 14 (1998) 8–16.
[3] Y. Kawaguchi, T. Segawa, Z. Feng, P. Li, Experimental study on drag-reducing channel flow with surfactant additives – spatial structure of turbulence investigated by PIV system, Int. J. Heat Fluid Flow 23 (2002) 700–709.
[4] N.K.-R. Kevlahan, Rapid distortion of turbulent structures, Appl. Sci. Res. 51 (1993) 411–415.
[5] F.-C. Li, Y. Kawaguchi, K. Hishida, M. Oshima, Investigation of turbulence structures in a drag-reduced turbulent channel flow with surfactant additive by stereoscopic particle image velocimetry, Exp. Fluids 40 (2006) 218–230.
[6] F.-C. Li, Y. Kawaguchi, T. Segawa, K. Hishida, Reynolds-number dependence of turbulence structures in a drag-reducing surfactant solution channel flow investigated by particle image velocimetry, Phys. Fluids 17 (2005) 075104.
[7] F.-C. Li, Y. Kawaguchi, K. Hishida, M. Oshima, On turbulent contribution to frictional drag in wall-bounded turbulent flow, Chin. Phys. Lett. 23 (2006) 1226–1229.
[8] C.R. Smith, J.D.A. Walker, A.H. Haidari, U. Sobrn, On the dynamics of near-wall turbulence, Philos. Trans. Royal Soc. London A336 (1991) 131–152.
[9] J. Zhou, R.J. Adrian, S. Balachandar, T.M. Kendall, Mechanisms for generating coherent packets of hairpin vortices in channel flow, J. Fluid Mech. 387 (1999) 353–396.
[10] R.J. Adrian, C.D. Meinhart, C.D. Tomkins, Vortex organization in the outer region of the turbulent boundary layer, J. Fluid Mech. 422 (2000) 1–54.
[11] K.T. Christensen, R.J. Adrian, Statistical evidence of hairpin vortex packets in wall turbulence, J. Fluid Mech. 431 (2001) 433–443.
[12] C.D. Tomkins, R.J. Adrian, Spanwise structure and scale growth in turbulent boundary layer, J. Fluid Mech. 490 (2003) 37–74.
[13] R.J. Adrian, B. Balachandar, Z.C. Liu, Spanwise growth of vortex structure in wall turbulence, KSME Int. J. 15 (2001) 1741–1749.
[14] M.R. Head, P. Bandyopadhyay, New aspects of turbulent boundary-layer structure, J. Fluid Mech. 107 (1981) 297–338.
[15] E.R. Corino, R.S. Brodkey, A visual study of turbulent shear flow, J. Fluid Mech. 37 (1969) 1–26.
[16] H.T. Kim, S.J. Kline, W.C. Reynolds, The production of turbulence near a smooth wall in a turbulent boundary layer, J. Fluid Mech. 50 (1971) 133–160.
[17] T.S. Luchik, W.G. Tiederman, Turbulent structure in low-concentration drag-reducing channel flow, J. Fluid Mech. 190 (1988) 241–263.
[18] G.L. Donohue, W.G. Tiederman, M.M. Reischman, Flow visualization of the near-wall region in a drag-reducing channel flow, J. Fluid Mech. 56 (1972) 559–575.
[19] K. Fukagata, K. Iwamoto, N. Kasagi, Contribution of reynolds stress distribution to the skin friction in wall-bounded flows, Phys. Fluids 14 (2002) L73–L76.
[20] Y. Kawaguchi, J. Wei, B. Yu, Z. Feng, Rheological characterization of drag-reducing cationic surfactant solution – shear and elongational viscosities of dilute solutions, in: Proceedings of the Fourth ASME–JSME Joint Fluids Engineering Conference, 2003, FEDSM2003-45653.
[21] R.J. Adrian, K.T. Christensen, Z.C. Liu, Analysis and interpretation of instantaneous turbulent velocity fields, Exp. Fluids 29 (2000) 275–290.
[22] J. Kim, P. Moin, R. Moser, Turbulence statistics in fully developed channel flow at low reynolds number, J. Fluid Mech. 177 (1987) 133–166.
[23] Y. Nagano, M. Tagawa, Statistical characteristics of wall turbulence with a passive scalar, J. Fluid Mech. 196 (1988) 157–185.
[24] F.-C. Li, Y. Kawaguchi, K. Hishida, Structural analysis of turbulent transport in a heated drag-reducing channel flow with surfactant additives, Int. J. Heat Mass Transfer 48 (2005) 965–973.